



## Probing molecular interactions with methylene blue derivatized self-assembled monolayers



Eleni Koutsoumpeli<sup>a</sup>, James Murray<sup>b</sup>, Dylan Langford<sup>a</sup>, Robin S. Bon<sup>b</sup>, Steven Johnson<sup>a,\*</sup>

<sup>a</sup> Department of Electronics, University of York, Heslington, York YO10 5DD, UK

<sup>b</sup> School of Chemistry, University of Leeds, Leeds LS2 9JT, UK

### ARTICLE INFO

#### Article history:

Received 23 June 2015

Received in revised form 4 September 2015

Accepted 7 September 2015

Available online xxxx

#### Keywords:

Biosensors

Redox monolayers

Self-assembled monolayers

### ABSTRACT

The emergence of stratified and personalised medicine and the associated need for highly multiplexed detection strategies are driving the development of innovative sensor technology. Electronic immunosensor arrays capable of label-free and highly parallel monitoring of ligand binding have emerged as a particularly promising technology capable of meeting these new diagnostic challenges. In this study, we present an approach for interrogating molecular interactions electronically using redox active molecular monolayers. Specifically, we have synthesised self-assembled molecular monolayers assembled from long-chain alkanethiols (LCAT) incorporating oligoethyleneglycol (OEG) linkers that can be derivatized with a range of functional groups, including the redox active molecule methylene blue. Critically, we show that the electron transport properties of this redox-active monolayer are highly sensitive to the electrochemical environment, including the local concentration of protons and the electrostatic potential at the plane of electron transfer. Using a combination of cyclic voltammetry and QCM-D to study in detail the behaviour of the monolayer during functionalisation and analyte binding, we demonstrate that these redox properties can be exploited for the electrochemical sensing of molecular interactions (biotin–avidin in our case) on SAMs. Given the versatility of LCAT-OEG monolayers, in terms of linker lengths, choice of functional group, and ability to create mixed component layers and the straight-forward assembly of mixed SAMs of high quality, our electrochemical sensing approach forms an excellent and generic label-free platform for probing a wide range of molecular interactions.

© 2015 The Authors. Published by Elsevier B.V. This is an open access article under the CC BY-NC-ND license (<http://creativecommons.org/licenses/by-nc-nd/4.0/>).

### 1. Introduction

Electrochemical immunosensor technologies enable label-free detection of molecular binding events between surface immobilised immuno-receptors, typically antibodies, and specific ligands in a sample matrix. The development of this hybrid technology not only requires robust and label-free approaches to transduce molecular binding events into a quantitative, electronic signal, but also integration solutions that ensure binding affinity, specificity and selectivity are retained following immobilization of immuno-receptors onto electronically active surfaces. In this manuscript we demonstrate a mixed self-assembled monolayer that contains both a redox-active component and chemically functional groups that addresses simultaneously the two challenges of electronic transduction and molecular immobilization.

We have recently demonstrated an efficient methodology for the synthesis of self assembled monolayers (SAMs) based on thiolated

long-chain alkanethiols (LCAT) incorporating oligoethyleneglycol (OEG) linkers of variable length [1]. LCAT-OEGs have been shown to be ideally suited for integrating immuno-receptors with a sensor platform [2]. Here, the LCAT component ensures spontaneous assembly of an ordered and densely packed monolayer onto coinage metal electrodes, typically gold, while the OEG component is efficient at minimising non-specific adsorption of peripheral molecules contained in a complex sample matrix, such as a clinical sample. Our solid-phase synthesis approach is not only efficient but also highly versatile and can be used to create bespoke LCAT-OEGs of variable length and derivatized with a wide range of functional groups that allow tuning of surface chemistry and conjugation of a range of molecular and biomolecular components. For example we have demonstrated an amine derivatized LCAT-OEG (named LCAT-OEG-NH<sub>2</sub> and shown in Fig. 1(a)) to which we can covalently couple proteins and peptides, either pre- or post-monolayer assembly, via free amine or carboxylic acid groups exposed on a protein or peptide surface. We have exploited this monolayer to immobilize antibodies onto electrode surfaces and demonstrated that the biocompatibility and hydrophilicity of the OEG linker

\* Corresponding author.

E-mail address: [steven.johnson@york.ac.uk](mailto:steven.johnson@york.ac.uk) (S. Johnson).

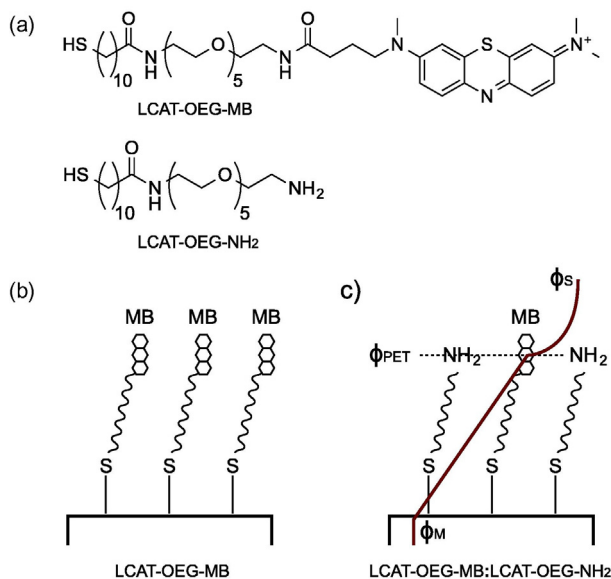


**Fig. 1.** (a) Chemical structure of LCAT-OEG-MB and LCAT-OEG-NH<sub>2</sub>. Details of the solid phase synthesis methodology can be found in Murray et al. [1]. (b) and (c) Schematic diagram of a 100% LCAT-OEG-MB monolayer and a mixed LCAT-OEG-MB : LCAT-OEG-NH<sub>2</sub> monolayer, respectively. (c) also illustrates the electrostatic potential profile in the mixed monolayer system. φ<sub>M</sub>, φ<sub>PET</sub> and φ<sub>S</sub> are the absolute potentials of the metal electrode, the plane of electron transfer and the bulk solution, respectively.

ensures antibody specificity and selectivity is preserved following immobilization [1].

Using the same methodology, we have also synthesized an innovative LCAT-OEG SAM derivatized with the redox active molecule methylene blue (named LCAT-OEG-MB and shown in Fig. 1) and that has been engineered specifically to act as a transduction element for monitoring molecular binding events electronically. Methylene blue (MB) is a heterocyclic aromatic chemical compound that is used widely as a dye, as a therapeutic for a range of medical conditions [5] and increasingly as a redox-active indicator for probing molecular interactions, particularly for the detection of DNA hybridisation [6] and for monitoring DNA aptamer binding [7]. The MB redox reaction is a two electron, one proton process described by the Nernst equation:

$$E = E^0 + \frac{RT}{2F} \ln \left[ \frac{\Gamma_o}{\Gamma_R} \right] + \frac{RT}{2F} \ln [H^+] \quad (1)$$

$E$  is the applied potential and  $\Gamma_o$  and  $\Gamma_R$  are the concentration of surface immobilized oxidised and reduced methylene blue, respectively. The formal potential,  $E^0$ , is given by:

$$E^0 = E^0 + \phi_{PET} - \phi_S \quad (2)$$

Here,  $E^0$  is the standard electrode potential,  $\phi_{PET}$  is the potential at the plane of electron transfer i.e. the plane in which the electroactive molecule lies, and  $\phi_S$  is the solution potential (see Fig. 1(c)). From these equations it is clear that at a fixed ionic strength, i.e. constant  $\phi_S$ , a change in local pH or in  $\phi_{PET}$ , for example due to binding of a charged protein at the plane of electron transfer, will lead to a shift in the formal potential, providing a mechanism to transduce molecular binding into a quantitative, electronic signal.

In this manuscript, we demonstrate a mixed molecular monolayer that consists of LCAT-OEG-MB and LCAT-OEG-NH<sub>2</sub> components where the NH<sub>2</sub> component acts as a scaffold for the covalent immobilization of immuno-receptors, and the MB is an indirect probe of molecular

interactions. Here, binding of a target ligand to the immobilised immuno-receptor leads to a change in the electrostatic environment local to the MB leading to a quantitative, electrochemical measurement of the molecular interaction. Unlike other similar proposals, Ho et al. [3, 4] our approach based on LCAT-OEG SAMs provide a number of significant benefits, including; immobilisation and sensing in a single bio-compatible, stable and anti-fouling monolayer; access to a variety of surface chemistries for the integration of a wide range of small molecules/immuno-receptors; simple and precise control over the ratio of components assembled in the mixed monolayer, providing a facile approach for regulating the surface density of immuno-receptors; precise control of the length of both the LCAT and OEG components and thus the location of the MB sensing component relative to the immobilized immuno-receptors.

## 2. Materials and methods

### 2.1. Materials

N-18-(N-(carboxypropyl) methylene blue)-3,6,9,11,15-pentaoxaheptadecyl-11-mercaptopundecanamide and N-18-amino-3,6,9,11,15-pentaoxaheptadecyl-11-mercaptopundecanamide (referred to as LCAT-OEG-MB and LCAT-OEG-NH<sub>2</sub> respectively) were synthesised as described by Murray et al., [1] and stored in ethanol at 10 mM concentration. All buffers were prepared using ultrapure water (18.2 MΩ cm, Milli-Q systems) and the pH confirmed using a pH metre (Mettler-Toledo, Switzerland). Chemicals were purchased from Sigma-Aldrich (Gillingham, UK) unless otherwise noted.

### 2.2. Cyclic voltammetry (CV)

Single component and mixed LCAT-OEG monolayers were immobilized on planar gold surfaces fabricated by electron beam evaporation of 25 nm Ti/100 nm Au onto a cleaned Si wafer (IDB technologies, Wiltshire, UK). Prior to functionalization, the wafers were cleaved and cleaned by immersion in piranha solution for 10 min (7:3 H<sub>2</sub>SO<sub>4</sub>, H<sub>2</sub>O<sub>2</sub>. Caution: piranha solution is very dangerous, being both strongly acidic and a strong oxidizer), followed by sonication in water, ethanol and isopropyl alcohol (IPA) for 10 min each. Functionalization of the Au surface with 100% LCAT-OEG-MB was achieved by immersion in a 0.2 mM ethanolic solution for 48 hours. Similarly, mixed SAMs were formed by immersion in ethanolic solutions containing equal volumes of 0.2 mM LCAT-OEG-MB and 0.2 mM LCAT-OEG-NH<sub>2</sub> for 48 hours. Cyclic voltammetry was performed using a Bio Logic VSP300 potentiostat. The functionalized Au working electrode was mounted in a three electrode electrochemical cell containing a Pt counter electrode and Ag/AgCl (saturated KCl) reference electrode. Contact to the working electrode was via a spring loaded pin connector. The surface area exposed by the electrochemical cell was defined by a Viton O-ring and was equal to 9.1 mm<sup>2</sup>.

### 2.3. Quartz crystal microbalance with dissipation monitoring (QCM-D)

Electrochemical QCM-D (EQCM-D) (QSense E4, electrochemistry module, QEM 401, Biolin Scientific, Stockholm, Sweden) was used to enable simultaneous monitoring of molecular binding with electrochemical measurements of the MB redox process *in situ*. This combination of techniques provides critical insight into the structure of the local molecular layer and thus a better understanding of the mechanisms that regulate interfacial electron transfer. Gold coated QCM-D sensors (QSX 338, Biolin Scientific, Stockholm, Sweden) were first cleaned by sonication in 1% Hellmanex followed by thorough rinsing in water and UV-ozone treatment for 30 min. Cleaned sensors were loaded into the EQCM-D module. This module includes a stainless steel counter electrode, a low leak Ag/AgCl reference electrode and contact to the Au working electrode. The surface area exposed to the electrolyte was equal to

1.13 cm<sup>2</sup> as defined by a Viton O-ring. A running buffer of 100 mM phosphate buffer (pH7) was passed over the sensor surface at a flow rate of 100  $\mu\text{L min}^{-1}$  until a steady baseline was reached.

Functionalisation of the sensor surface with a mixed LCAT-OEG SAM was achieved *in situ* by exposure to an aqueous solution containing equal volumes of 0.2 mM LCAT-OEG-MB and 0.2 mM LCAT-OEG-NH<sub>2</sub> at a flow rate of 20  $\mu\text{L min}^{-1}$  for 60 min before returning to running buffer at a flow rate of 50  $\mu\text{L min}^{-1}$ . Free amines exposed by the LCAT-OEG-NH<sub>2</sub> were functionalised with biotin using a 1 mM aqueous solution of EZ-Link NHS-Biotin (Thermo Fisher Scientific, Rockford, USA) which was passed over the sensor surface at 50  $\mu\text{L min}^{-1}$  for 15 min. Finally, the biotin functionalised surface was exposed to avidin at 1 mg/mL in phosphate buffer (100 mM, pH 7) at a flow rate of 50  $\mu\text{L min}^{-1}$  for 400 s before again returning to running buffer. Cyclic voltammetry was performed between each stage of surface modification using a Bio Logic VSP300 potentiostat with a Ag/AgCl reference electrode and stainless steel counter electrode built into the electrochemical QCM-D cell.

### 3. Results and discussion

#### 3.1. Redox activity of LCAT-OEG-MB monolayers

A typical cyclic voltammogram of a monolayer of LCAT-OEG-MB assembled on a gold electrode is shown in Fig. 2(a) and in (b) where the non-Faradaic capacitive charging current has been removed. Measurements were performed in 100 mM phosphate buffer at pH 7.2. The oxidation and reduction peaks are highly symmetric and exhibit very small peak splitting,  $\Delta E_{pk}$ , at low scan rates (e.g.  $\Delta E_{pk} = 9$  mV at a scan rate of 200  $\text{mVs}^{-1}$  as in Fig. 2(a) and (b)) consistent with an ideal, reversible and surface immobilized redox system. The formal potential,  $E^0$ , at pH 7.2 is  $-128$  mV versus Ag/AgCl. We note, this is significantly smaller than formal potential observed in ferrocene-terminated monolayers and reduces the potential for voltage-induced damage of the LACT-OEG-MB monolayer. The full width at half maximum (FWHM) of the oxidation and reduction peaks, 65 mV and 70 mV respectively, is larger than the ideal 45.3 mV of a two-electron process. Deviations from the ideal FWHM is observed frequently in immobilised redox systems and often attributed to electrostatic interactions between neighbouring charged groups within the SAM. Here, from the linearity between peak current and voltage scan rate [8], Fig. 2(c), we estimate the surface coverage of LCAT-OEG-MB is  $4 \times 10^{12}$  molecules/cm<sup>2</sup>. This is lower than the density of an ideal LCAT SAM [9], likely due to steric interference from the oligoethyleneglycol and MB tail groups, but still suggests close packing between adjacent SAM molecules. Moreover, the high flexibility of the oligoethyleneglycol component is expected to lead to a wide distribution in the distance between the MB and the electrode, leading to further broadening of the peaks.

The electron transfer rate,  $k_{ET}$ , as calculated from the Laviron plot [8] of Fig. 2(d) is  $10.4 \text{ s}^{-1}$ . This is comparable to the rate of electron tunnelling observed using ferrocene-LCAT monolayers on gold consisting of 17 alkane units [10]. We note however that the spatial distribution of methylene blue and coupling between neighbouring redox sites limits the accuracy of  $k_{ET}$  calculation. Finally, and critically for future applications in biological sensing, the electrochemical characteristics of the LCAT-OEG-MB monolayer are highly repeatable and stable in aqueous solutions with no notable change even after storage in phosphate buffer for 5 days.

##### 3.1.1. Redox activity of LCAT-OEG-MB monolayers: pH dependency

Cyclic voltammograms of the LCAT-OEG-MB monolayer as a function of buffer pH are shown in Fig. 3(a). The potential for oxidation and reduction is seen to shift to increasingly negative values with increasing pH (decreasing proton concentration), in agreement with the Nernst equation (Eq. (1)). We note, the shift in peak potential as a result

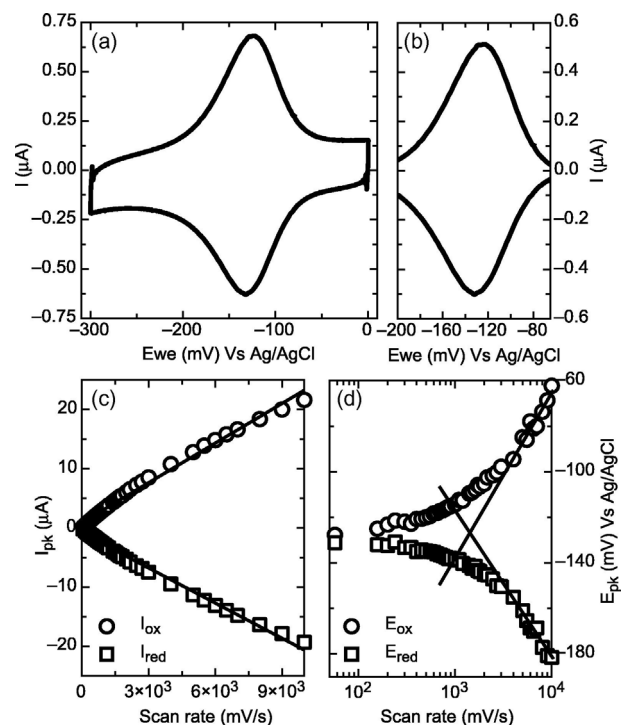


Fig. 2. (a) Typical CV using a voltage scan rate of 200  $\text{mVs}^{-1}$  for a 100% LCAT-OEG-MB monolayer assembled on an Au electrode and (b) following removal of the capacitive charging current. (c) Change in peak oxidation,  $I_{ox}$ , and peak reduction current,  $I_{red}$ , as a function of voltage scan rate,  $\nu$ . (d) Laviron (trumpet) plot showing fit to linear regions at high scan rates. All measurements were performed in 100 mM phosphate buffer at pH 7.2.

of changes in pH is reversible however exposure of the LCAT-OEG-MB SAM to highly acidic solutions ( $\leq \text{pH } 2$ ) leads to irreversible damage of the LCAT-OEG-MB SAM and a loss in redox activity.

The rate at which the formal potential shifts due to changes in pH over the range pH 4 and 12 is found to be  $-33$  mV/pH, as shown by the straight line fit to the data in Fig. 3(b). This is very close to the ideal Nernstian pH dependence of  $-30$  mV/pH predicted for a 2 electron, 1 proton redox process. Although the pH dependent behaviour follows expected Nernstian behaviour, it is important to verify that the observed response is attributable to the local proton concentration, rather than restructuring of the LCAT-OEG-MB monolayer due to changes in pH. This was confirmed by QCM-D measurements that indicated the conformation of the monolayer remains constant between pH 5–8 (data not included).

In a previous study of methylene blue intercalated with a DNA monolayer, Ceres et al. [11] observed a non-linear dependency between redox potential and pH when characterised in phosphate buffer. This non-linearity was related to the differential permeability of mono- and divalent phosphate ions within the charged DNA film. The Nernstian pH dependence observed here for the LCAT-OEG-MB monolayer suggests no such solution effects, suggesting a continuous and equal distribution of ions within the oligoethylene glycol component of the monolayer.

In addition to a shift in the formal potential with pH, we also observe a pH dependent change in the peak current, as shown in Fig. 3(a). In particular the peak current reduces with reducing pH over the range pH 4–8. This shift in current is related to a change in the electron transfer rate,  $k_{ET}$ , as calculated from the Laviron plots of Fig. 3(c) which reduces from  $k_{ET} = 10.4 \text{ s}^{-1}$  at pH 7.0 to  $k_{ET} = 8 \text{ s}^{-1}$  at pH 4. This reduction in  $k_{ET}$  is related to the change in the kinetics associated with protonation/deprotonation of the methylene blue.

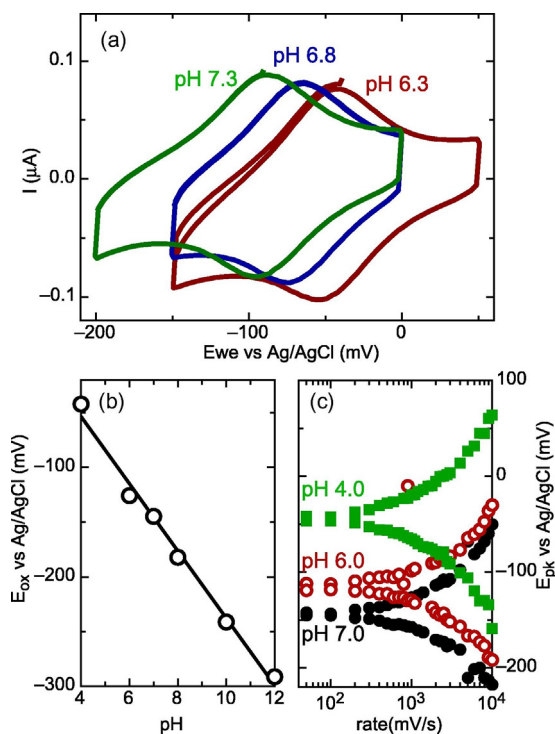


**Fig. 3.** (a) Typical CV characteristics as a function of buffer pH for a 100% LCAT-OEG-MB monolayer assembled on an Au electrode at a voltage scan rate of  $50 \text{ mVs}^{-1}$ . (b) Shift in potential of the LCAT-OEG-MB oxidation peak as a function of pH. (c) Laviron plot of a function of buffer pH. All measurements were performed in 100 mM phosphate buffer.

### 3.1.2. Redox activity of LCAT-OEG-MB monolayers: $\phi_{\text{PET}}$ dependency

Having established the dependencies between the electron transfer process and pH, we next examined the shift in formal potential due to a change in the potential at the plane of electron transfer,  $\phi_{\text{PET}}$  (see Eq. (2)). To investigate the sensitivity of LCAT-OEG-MB to local changes in  $\phi_{\text{PET}}$ , we created a mixed molecular monolayer assembled from LCAT-OEG-MB and LCAT-OEG-NH<sub>2</sub> (see schematic of Fig. 1(c)) where the charge associated with the NH<sub>2</sub>-terminated dilutant modifies  $\phi_{\text{PET}}$  at the same plane as the MB. Fig. 4 shows the formal potential of LCAT-OEG-MB in the presence of co-immobilised amine-terminated LCAT-OEG over a pH range 5.5–8. Critically, in the presence of the protonated (i.e. positively charged) NH<sub>2</sub>-terminated dilutant, we observe a shift in the formal potential with electron transfer now occurring at an increasingly positive potentials, in agreement with the Nernst equation. The linear pH dependency observed for the 100% LCAT-OEG-MB SAM is maintained for the diluted SAMs and yields a shift in the formal potential of  $-35 \text{ mV/pH}$ , again close to the ideal Nernstian response.

### 3.2. Label-free detection of molecular interactions using LCAT-OEG-MB

Above we have confirmed that the redox activity of methylene blue is preserved when assembled onto an electrode surface in a molecular monolayer of LCAT-OEG-MB and that the formal potential retains its sensitivity to the local charge,  $\phi_{\text{PET}}$ , and pH, as predicted by the Nernst equation. In addition to changes in energetics, previous studies have also shown that the kinetics of interfacial electron transfer are sensitive to the local environment. For example the rate of electron transfer for ferrocene groups embedded (buried) within a SAM has been shown to be significantly reduced due to limited ion diffusion from the bulk electrolyte to the buried ferrocenes [12]. ‘Ion-gated electron transport’ has also been observed in buried azobenzene units that were found to be immune to reduction even when the applied potential was sufficient

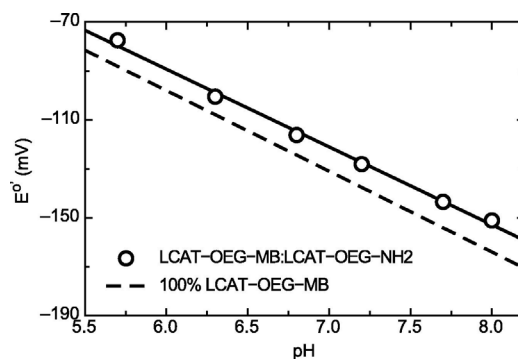


**Fig. 4.** Formal potential for a 100% LCAT-OEG-MB and a mixed monolayer of LCAT-OEG-MB:LCAT-OEG-NH<sub>2</sub> as a function of electrolyte pH. Lines show linear fit to data.

to bring about oxidation or reduction [13]. In addition to local solvent effects, the electrochemical double layer potential, SAM capacitance and lateral displacement of the redox centres each play a role in the electron transfer process, regulating the formal potential, the voltammetric peak current and peak width [14].

Our mixed LCAT-OEG SAMs enable us to exploit these sensitivities to transduce molecular binding events into an electronic signal. We previously developed and demonstrated the LCAT-OEG-NH<sub>2</sub> SAM as a biologically compatible, anti-fouling monolayer for covalently immobilizing functional proteins onto electrode surfaces. We now combine this approach for electrode derivitization with the environmental sensitivity of LCAT-OEG-MB to monitor local molecular interactions. Here, mixed monolayers of LCAT-OEG-MB:LCAT-OEG-NH<sub>2</sub> are assembled on an electrode surface, as in Fig. 1(c). Amines exposed by the LCAT-OEG-NH<sub>2</sub> component can be used to conjugate and localise (bio)molecules close to the MB. Any subsequent change in the local environment, for example due to binding to the immobilized receptor, can be detected directly (i.e. label-free) by the corresponding change in the MB redox process.

In the first case, we have chosen to employ the well studied and high affinity biotin-avidin system, in which the mixed LCAT-OEG-MB:LCAT-OEG-NH<sub>2</sub> monolayer is functionalized with biotin coupled to an amine-reactive NHS ester. In order to gain greater insight into the label-free detection mechanism, we employed EQCM-D [15] that permits acoustic-wave measurements of molecular binding in parallel with electrochemical characterisation of the MB redox process. The QCM-D data not only provides an independent measure of molecular binding, but critically can also reveal information regarding the conformation of the surface-immobilized molecular construct and thus insight into the environment local to the MB. Real-time QCM-D data resulting from the assembly of a mixed LCAT-OEG-MB:LCAT-OEG-NH<sub>2</sub> monolayer directly on the cleaned Au sensors is shown in Fig. 5(a). The resonant frequency for each of the harmonics (only the third harmonic,  $F_3$ , is shown here) is seen to decrease indicating an increase in mass deposited on the sensor surface, consistent with the assembly of a molecular layer. The change in frequency,  $\Delta f$ , saturates after around 60 min at which time  $\Delta f$  is  $-35 \text{ Hz}$ . This shift in frequency corresponds to an estimated deposited mass of  $194.7 \text{ ng/cm}^2$ , as calculated using the Sauerbrey equation. Assuming an average molecular weight of the LCAT-OEG-MB ( $\text{MW} = 818.4 \text{ g/mol}$ ) and LCAT-OEG-NH<sub>2</sub> ( $\text{MW} = 480.33 \text{ g/mol}$ ) monolayer of  $649.4 \text{ g/mol}$ , this shift in mass is equivalent to a molecular layer consisting of  $1.8 \times 10^{14}$  molecules/cm<sup>2</sup>. This is comparable to the density of a well packed, LCAT monolayer [9] but larger than that calculated above for a 100% LCAT-OEG-MB monolayer. We note, the linear relationship between adsorbed mass and  $\Delta f$  described by the Sauerbrey equation does not account for damping effects due to the viscosity of the molecular layer and surrounding solution. Our calculation is thus likely to be an overestimate of the actual molecular surface density. The use of EQCM-D also enabled us to confirm the redox activity of

the assembled monolayer *in situ*. A typical cyclic voltammogram of the LCAT-OEG-MB monolayer is shown in Fig. 5(d) measured using a 100 mM phosphate buffer, pH 7 supporting electrolyte.

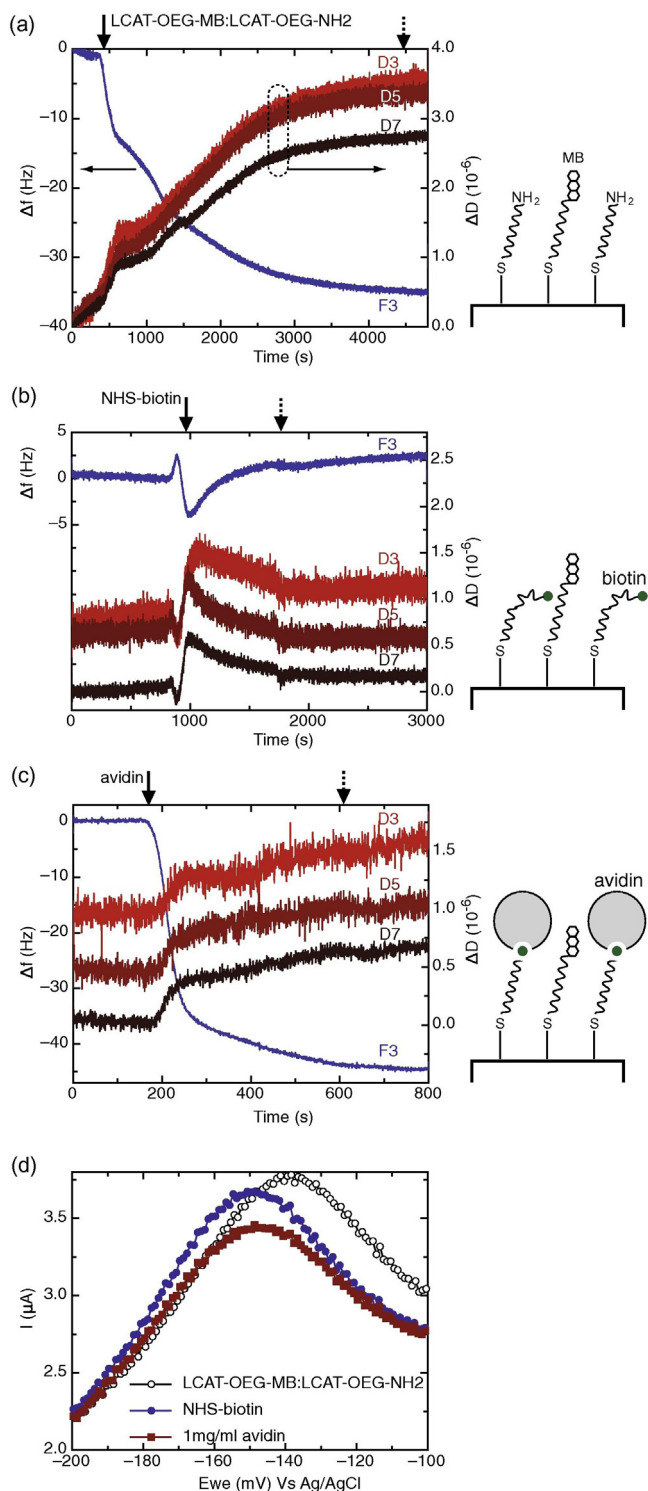


**Fig. 5.** Real time QCM-D showing shift in resonant frequency,  $\Delta f$ , and dissipation,  $\Delta D$ , during (a) assembly of mixed LCAT-OEG-MB: LCAT-OEG-NH<sub>2</sub> on Au-coated QCM-D sensor surface, (b) monolayer functionalization using biotin coupled to an amine-reactive NHS ester and (c) following exposure to avidin at 1 mg/mL. The start and end of each functionalization stage are indicated by solid and broken respectively.  $F_n$  and  $D_n$  denote the frequency (F) and dissipation (D) of the  $n$ th harmonic. (d) Cyclic voltammograms of the MB oxidation peak taken *in situ* at each stage of surface functionalization.

The decrease in frequency resulting from the formation of the mixed monolayer is accompanied by a corresponding increase in the damping of the crystal oscillation,  $\Delta D$ , associated with the viscoelastic properties of the layer. The large shift in dissipation observed here suggests a layer with a greater viscosity than the bare Au sensor surface, as expected for the assembly of a molecular monolayer. The distance into solution over which the energy of the acoustic wave is dissipated is dependent on the acoustic frequency,  $f$ , and varies according to  $f^{-1/2}$  [16]. Higher order, and thus higher frequency harmonics decay more rapidly away from the surface and are consequently more sensitive to the viscoelastic properties of the near surface region. Here, the near surface region is dominated by the well-packed, LCAT component which is expected to be significantly less viscous than the upper, unstructured OEG layer. This difference in the viscoelasticity of the alkane and oligoethyleneglycol (OEG) monolayer components is reflected in the dissipation data. In particular, and as shown in Fig. 5(a),  $\Delta D$  for the lower order harmonics ( $\Delta D_3 = 3.6 \times 10^{-6}$  and  $\Delta D_5 = 3.4 \times 10^{-6}$  for the third and fifth harmonics respectively) is greater than observed for the higher order harmonics ( $\Delta D_7 = 2.8 \times 10^{-6}$  for seventh harmonic) consistent with a monolayer assembled from a well-packed, LCAT near surface region coupled to a viscous OEG component at the solution interface.

We next functionalized amines exposed by the LCAT-OEG-NH<sub>2</sub> monolayer component using biotin coupled to an amine-reactive NHS ester. Real time QCM-D data of biotin functionalization are shown in Fig. 5(b). Upon exposure to the NHS-biotin, the frequency is seen to initially decrease, consistent with the immobilization of biotin onto the amine-terminated surface before slowly increasing finally returning close to the initial resonant frequency. In order to understand this behaviour it is necessary to also monitor changes in the dissipation that occur during functionalisation. Here, we see a rapid increase in dissipation over the first 100 s of functionalization, followed by a slow recovery over the next 15 min. Such behaviour is commonly associated with conformational changes occurring within the molecular layer [17]. Furthermore,  $\Delta D$  after biotin functionalization becomes equally separated for all harmonics. This is in contrast to the behaviour of  $\Delta D$  observed for the LCAT-OEG-MB: LCAT-OEG-NH<sub>2</sub> monolayer, that displayed differences between the lower and higher order harmonics. This is again consistent with a conformational change induced by biotin binding and indicates homogeneous viscoelastic properties of the restructured SAM. We believe this conformational change reflects a restructuring of the OEG layer to screen the hydrophobic biotin from the surrounding aqueous solvent. This conformational change coupled with the local change in electrostatic charge (from positively charged, protonated amine groups to neutral biotin) results in a shift in the local potential at the plane of electron transport. This is reflected in a corresponding shift in the potential for MB oxidation, as shown in Fig. 5(d).

The biotin surface was next challenged with avidin at a concentration of 1 mg/mL. The high binding affinity associated with the avidin-biotin interaction leads to a significant increase in the mass immobilized on the surface, as seen by the shift in  $\Delta f$  in Fig. 5(c). The response saturates after around 400 s after which  $\Delta f = -50$  Hz, equivalent to a deposited mass of 295 ng/cm<sup>2</sup>. This is equivalent to an estimated surface coverage of  $2.5 \times 10^{12}$  avidin molecules/cm<sup>2</sup>. Following avidin binding, the oxidation potential of the MB changes moderately, increasing to more positive voltages as a result of the positive charge on the immobilized avidin (isoelectric point of avidin, pI = 10). In addition to a shift in potential, we also observe a reduction in the FWHM and, more significantly, the peak current which reduces by around 10%. A similar reduction in Faradaic current has been observed in Fc-SAMs in which the ferrocene is buried within a monolayer [12], where the reduced current is associated with a slowing of the kinetics of electron transfer due to limited access of screening ions from solution. Given the high surface coverage of avidin observed here, it is reasonable to expect a similar reduction in the rate of ion and/or proton diffusion, leading to the reduced rate of electron transfer.

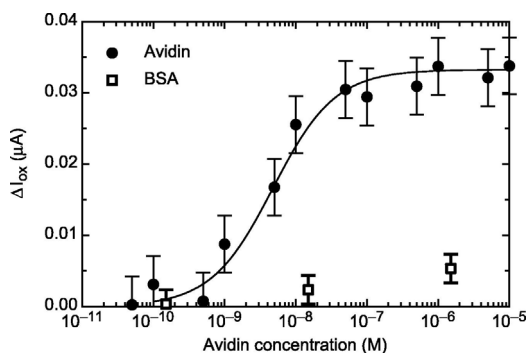


**Fig. 6.** Binding analysis of the biotin–avidin complex as monitored through changes in the peak oxidation current,  $\Delta I_{ox}$ , in co-immobilized LCAT-OEG-MB. The solid line shows Langmuir equation fit to data. Open symbols show  $\Delta I_{ox}$  measured following exposure to BSA.

Finally, we exposed LCAT-OEG-MB: LCAT-OEG-NH<sub>2</sub>-biotin layers to a series of different concentrations of avidin. Fig. 6 shows the change in peak oxidation current,  $\Delta I_{ox}$ , of the immobilized MB layer as a function of avidin concentration. The curve follows a clear Langmuir isotherm, as fit by the solid line in Fig. 6. Using this assay we were able to detect avidin binding over a dynamic range of three orders of magnitude and with a detection limit of around 1 nM. Control experiments designed to show the specificity of detection were performed by challenging a surface functionalized with LCAT-OEG-MB: LCAT-OEG-NH<sub>2</sub>-biotin mixed monolayer with bovine serum albumin (BSA) at a range of concentrations. We observed only small shifts in the peak oxidation current even up to a BSA concentration of 1.5  $\mu$ M, as shown in Fig. 6. The notable lack of non-specific surface interactions further supports our use of a OEG containing monolayer, which is known to be efficient at minimizing non-specific adsorption. We note, this assay has not been optimised and there is significant potential to increase the detection limit further, for example through regulation of the length (i.e. number of ethyleneglycol or alkane units) and relative concentration of the LCAT-OEG-MB and LCAT-OEG-NH<sub>2</sub> components assembled in the monolayer.

#### 4. Conclusions

Robust approaches for electronic transduction of molecular binding events are of significant interest for the development of innovative sensor technologies. We have engineered and demonstrated a range of long-chain alkanethiols incorporating oligoethyleneglycol linkers that can address this challenge. Specifically, we have demonstrated self-assembled molecular monolayers consisting of mixed components of LCAT-OEG-MB and LCAT-OEG-NH<sub>2</sub>. The NH<sub>2</sub> component acts as a chemoselective scaffold for the immobilization of a binding molecule local to the redox active MB while the OEG component inhibits non-

specific binding, maintaining specificity of the assay. Specific molecular binding events can be detected directly and label-free by monitoring the change in electron transport properties of MB due to the corresponding change in local electrochemical environment. Given the versatility of LCAT-OEG monolayers, in terms of linker lengths, choice of functional group, and ability to create mixed component monolayers of high quality, our electrochemical sensing approach could be extended for the detection of a range of clinically relevant analytes by local immobilization of specific and selective immuno-receptors, such as antibodies, aptamers and antibody-mimetics.

#### Conflict of interest

None declared.

#### Acknowledgements

This research was funded by the EU through the Marie Curie ITN CAPACITE project, Grant number 608014 (SJ and EK), the sponsor-id="http://dx.doi.org/10.13039/50110000266">EPSRC, Grant EP/J010731/1 (SJ and RSB), the University of York through an Institutional Equipment award (SJ), the Biomedical and Health Research Centre of the University of Leeds (RSB) and a Henry Ellison PhD Studentship (JM).

#### References

- [1] J. Murray, D. Nowak, L. Pukenas, R. Azhar, M. Guillorit, C. Wälti, K. Critchley, S. Johnson, R.S.J. Bon, *Mater. Chem. B* 2 (2014) 3741–3744.
- [2] K.L. Prime, G.M. Whitesides, *Science* 252 (1991) 1164–1167.
- [3] M.Y. Ho, P. Li, P. Estrela, S. Goodchild, P. Migliorato, *J. Phys. Chem. B* 114 (2010) 10661–10665.
- [4] M.Y. Ho, S. Goodchild, P. Estrela, D. Chu, P. Migliorato, *Analyst* 139 (2014) 6118–6121.
- [5] M. Wainwright, K.B.J. Crossley, *Chemotherapy* 14 (2002) 431–443.
- [6] S.O. Kelley, J.K. Barton, N.M. Jackson, M.B. Hill, *Bioconjugate Chem.* 8 (1997) 31–37; C.G. Pheaney, J.K. Barton, *Langmuir* 28 (2012) 7063–7070.
- [7] Y. Liu, N. Tuleouva, E. Ramanbulov, A. Revzin, *Anal. Chem.* 82 (2010) 8131–8136; G.S. Bang, S. Cho, B.-G. Kim, *Biosens. Bioelectron.* 21 (2005) 863–870; Y. Xiao, R.Y. Lai, K.W. Plaxo, *Nature Protoc.* 2 (2007) 2875–2880.
- [8] A.L. Eckermann, D.J. Feld, J.A. Shaw, T.J. Meade, *Coordination, Chem. Rev.* 254 (2010) 1769–1802.
- [9] H. Dubois, R.G. Nuzzo, *Annu. Rev. Phys. Chem.* 43 (1992) 437–463.
- [10] K. Weber, L. Hockett, S.J. Creager, *Phys. Chem. B* 106 (1997) 10706–10713.
- [11] D.M. Ceres, A.K. Udit, D. Hill, M.G. Hill, J.K.J. Barton, *Phys. Chem. B* 111 (2007) 663–668.
- [12] J.J. Sumner, S.E.J. Creager, *Phys. Chem. B* 105 (2001) 8739–8745.
- [13] D.J. Campbell, B.R. Herr, J.C. Hultheen, R.P. Van Duyne, C.A.J. Mirkin, *Am. Chem. Soc.* 118 (1996) 10211–10219.
- [14] C.P. Smith, H.S. White, *Anal. Chem.* 64 (1992) 2398–2405; S. Mukherjee, S. Bandyopadhyay, A. Dey, *Electrochim. Acta* 108 (2013) 624–633.
- [15] M.C. Dixon, *J. Biomol. Tech.* 19 (2008) 151–158; M.R. Deakin, D.A. Buttry, *Anal. Chem.* 61 (1989) 1147A–1154A.
- [16] N.-J. Cho, K.K. Kanazawa, J.S. Glenn, C.W. Frank, *Anal. Chem.* 79 (2007) 7027–7035.
- [17] N.-J. Cho, C.W. Frank, B. Kasemo, F. Höök, *Nat. Protoc.* 5 (2010) 1096–1106.